Journal of Molecular Catalysis A: Chemical 327 (2010) 51–57

Contents lists available at ScienceDirect

Journal of Molecular Catalysis A: Chemical

journal homepage: www.elsevier.com/locate/molcata

Enhancement of photocatalytic oxidation of oxalic acid by gold modified WO_3/TiO_2 photocatalysts under UV and visible light irradiation

V. Iliev[a,*], D. Tomova[a], S. Rakovsky[a], A. Eliyas[a], G. Li Puma[b]

[a] Institute of Catalysis, Bulgarian Academy of Sciences, 1113 Sofia, Bulgaria
[b] Photocatalysis & Photoreaction Engineering, Department of Chemical and Environmental Engineering, Faculty of Engineering, The University of Nottingham, University Park, Nottingham NG7 2RD, United Kingdom

ARTICLE INFO

Article history:
Received 30 March 2010
Received in revised form 14 May 2010
Accepted 17 May 2010
Available online 24 May 2010

Keywords:
TiO_2
WO_3
Composite photocatalysts
Gold
Oxalic acid
UV–vis light irradiation

ABSTRACT

The photooxidation of oxalic acid, catalyzed by nanosized TiO_2 or WO_3 and composite photocatalysts: Au/TiO_2, Au/WO_3, WO_3/TiO_2, $Au/WO_3/TiO_2$ was studied under irradiation with UV, visible and combined UV–visible light. The catalysts were characterized by the XRD, XPS, SEM and TEM methods. The photocatalytic mineralization of oxalic acid, catalyzed by WO_3/TiO_2 or $Au/WO_3/TiO_2$, proceeded at a significantly higher rate under UV-A irradiation than that under visible light. This is due to the lower specific surface area of the WO_3 and its small amount in the composite catalyst. Doping of the semiconductor materials with gold nanoparticles more than doubles the rates of mineralization of oxalic acid, compared to the un-doped samples, and more significantly in the case of $Au/WO_3/TiO_2$. The higher rate constants of oxalic acid decomposition under UV, visible or UV–visible light irradiation with the WO_3/TiO_2 and $Au/WO_3/TiO_2$ catalysts, compared with those measured with the individual oxide photocatalysts, are due to the more efficient separation of the electron–hole charges generated upon irradiation. Especially efficient is the charge separation in the case of the $Au/WO_3/TiO_2$ photocatalyst under irradiation with UV or combined UV–visible light, when the rate constants of oxalic acid destruction are approximately 1.7 times higher than that of the process catalyzed by Au/TiO_2 and 3 times higher than that catalyzed by pure TiO_2.

1. Introduction

Photocatalytic reactions on semiconductor materials, irradiated with solar or artificial light, are of great interest because of their applicability for the removal of a large variety of pollutants, both in aqueous and in gaseous phase [1–7]. Band-gap excitation of a semiconductor produces photoinduced electrons and holes, which can respectively reduce and oxidize species, adsorbed on the surface of semiconductor particles [8]. However, a major disadvantage in most semiconductor materials is the high degree of recombination between the photogenerated charge carriers, which ultimately decreases the photocatalyst effectiveness and the photonic efficiency of the redox process. Titanium dioxide (TiO_2) is one of the most widely recognised semiconductor photocatalyst, triggering off the oxidative destruction and mineralization of a wide range of organic substrates. The processes of catalytic oxidative destruction with TiO_2 are accomplished under UV light irradiation, due to the wide band gap of the anatase form of TiO_2 (3.2 eV). Sunlight may conveniently be used as the source of photon energy, however, the fraction of UV light in the solar energy radiation spectrum is only about 4%. During the last years, studies in the field of photocatalysis have therefore focused on the preparation of semiconductor materials capable of utilizing, effectively, both the UV and the visible component of solar light. The aim has been to increase the photonic efficiency of the processes of destruction of water and air contaminants [9–11]. In consequence, single semiconductor materials [12–14] have been studied, as well as, doped semiconductors [13–15] or coupled semiconductors systems, in which one of them is excited by visible light irradiation (organic or inorganic semiconductors) [12,13,15–20]. Another approach to promote the photonic efficiency of a semiconductor photocatalyst has been the surface modification with nanosized particles of noble metals [18,21–23].

A number of authors have investigated coupled WO_3/TiO_2 systems under illumination with UV [24–27] or visible light [28–30] with the purpose of promoting the photonic efficiency of TiO_2 in the decomposition of water and air contaminants. WO_3 is a semiconductor photocatalyst with a band gap of 2.8 eV, which is activated by visible light illumination. The basic disadvantage of WO_3 as a photocatalyst is its low photonic efficiency. It has been reported [26,27,30], that the activity of WO_3/TiO_2 photocatalysts, under UV light irradiation, is highest at an optimum WO_3 content in the composite material of about 3–4 wt%. The promoting effect of noble metals (in particular gold) on the WO_3/TiO_2 system efficiency, has received little attention so far in the literature.

* Corresponding author. Tel.: +359 2 9792514; fax: +359 2 9712967.
E-mail address: iliev@ic.bas.bg (V. Iliev).

1381-1169/$ – see front matter © 2010 Elsevier B.V. All rights reserved.
doi:10.1016/j.molcata.2010.05.012

In this work, the photocatalytic oxidation of oxalic acid, catalyzed by WO_3, TiO_2 and WO_3/TiO_2 and of the corresponding gold (Au^0) modified materials, Au/WO_3, Au/TiO_2 and $Au/WO_3/TiO_2$ was compared under UV, visible (vis) and combined UV–vis irradiation. The basic aim of this study was to elucidate the influence of Au^0 on the composite WO_3/TiO_2 material and evaluate the enhancement of the oxidation rates of oxalic acid (model organic substrate) under UV–vis irradiation.

2. Experimental

2.1. Materials and preparation of photocatalysts

TiO_2 (Degussa, P25) was used as the starting photocatalytic material. Tungstic acid, H_2WO_4 (Aldrich), hydrogen tetrachloroaurate(III) $HAuCl_4{\cdot}3H_2O$ (Aldrich) and oxalic acid HO_2CCO_2H (Aldrich) were used as received, without further purification.

TiO_2 was coated with nanosized WO_3 particles (4 wt%) following the method in reference [31] with further modifications. Aqueous ammonia solution was initially added to a mixture of 0.216 g H_2WO_4 in 10 ml of water until the tungstic acid was completely dissolved. Further 5 g of TiO_2 was added under continuous stirring. The obtained mixture was stirred for 30 min and then acidified to pH 4 using 0.5 M hydrochloric acid (Aldrich). 10 ml of an aqueous solution of oxalic acid (0.1 M) was then added to the mixture and stirred for a further hour at 40 °C. The role of oxalic acid was to prevent the aggregation of WO_x particles in the precipitate – to obtain more uniform distribution of smaller amorphous WO_x particles on the TiO_2 surface [31]. Finally, the solid product was dried at 383 K for 2 h and calcined at 693 K for two further hours. Pure nanosized WO_3 was prepared following the same methodology using H_2WO_4 as the precursor.

The gold-loaded semiconductor materials (0.4 wt% noble metal loading on the supports) were synthesized by the photoreduction method [21,22]. This amount of noble metal was selected based on previous investigations, which reported to be optimal [21]. The method was as follows. For each metallized sample, 5 g of TiO_2 was dispersed into 500 ml solution of $HAuCl_4{\cdot}3H_2O$ (0.1 mmol) in bi-distilled water. Upon anchoring the Au onto TiO_2, methanol was added as a sacrificial donor at a molar ratio of methanol to noble metal salts equal to 500:1. The pH of the suspensions was adjusted to 7 by adding a buffer solution (Fixanal, Fluka). Varying the pH, it has been reported that the Au^0 nanoparticle size was the smallest in the case of photoreduction at pH = 7, whereupon the activity of the photocatalyst was the highest [22]. For this reason the same pH = 7 was also used for the surface modification with gold of the pure WO_3 and WO_3/TiO_2 composite. The reaction system was stirred continuously at room temperature under nitrogen bubbling (100 ml/min) to remove oxygen from the solution. Bubbling was carried out for a short time interval (15 min) to avoid undesirable consecutive reactions at these pH values [22,32,33]. The suspension under continuous stirring was irradiated for 3 h by a UV-C lamp (Philips, TUV 4W) emitting radiation at 253.7 nm, to reduce Au^{3+} to its metallic state Au^0. Finally, the precipitate was washed with bi-distilled water and then dried at 383 K for 12 h.

2.2. Characterization of the photocatalysts

BET surface areas of specimens were measured by nitrogen adsorption at the liquid nitrogen boiling temperature using a Micromeritics FlowSorb II 2300 apparatus based on adsorption data in the partial pressure (P/P_0) range of 0.05–0.35.

The adsorption of oxalic acid on the pure TiO_2, WO_3, composite WO_3/TiO_2 and gold modified semiconductor materials was measured at pH = 4, the pH used during the photocatalytic experiments. In each experimental run, 350 mg of photocatalytic material was added to 350 ml of an aqueous oxalic acid solution (1.8×10^{-2} mol/L). The suspension was then magnetically stirred for 60 min at 293 K, in the dark and in the absence of oxygen to reach adsorption/desorption equilibrium [34]. The photocatalytic material was then separated by filtration (Whatman, Grade 42). The residual oxalic acid concentration in the filtrate was measured by a total organic carbon (TOC) analyzer (Shimadzu VCSH) to calculate the amount of oxalic acid adsorbed on each catalyst sample.

The diffuse reflectance spectra of TiO_2, WO_3 and WO_3/TiO_2 powders were recorded on UV–vis spectrometer JASCO V-570 to characterize the spectral features of the photocatalyst samples and to determine semiconductor band-gap energies.

The crystal phase of WO_x was identified by X-ray diffraction (XRD) measurements which were carried out at room temperature using a Rigaku D/MAX-IIIA diffractometer with Cu Kα radiation ($\lambda = 0.15418$ nm).

X-ray photoelectron spectroscopy (XPS) measurements were performed with a VG ESCALAB MK II spectrometer under UHV conditions (base vacuum: $\sim 10^{-8}$ Pa). Mg Kα radiation was used as the X-ray source. The carbon 1s line (with binding energy of 284.8 eV) was used to calibrate the binding-energy scale of the XPS.

The morphological and structural differences of both WO_3 and WO_3/TiO_2 were observed by a scanning electron microscope (SEM) (JEOL model JSM-5300). The WO_3 crystallite size was determined by TEM (JEOL JEM 100B). The size distribution of Au nanoparticles on the photocatalysts was examined with a HRTEM (JEOL JEM-3011) operated at 300 keV, equipped with a PGT energy-dispersive X-ray (EDX) solid-state detector making use of Excalibur software. The average metal particle size was determined statistically based on the sizes of at least 100 particles.

2.3. Photocatalytic experiments

The photodegradation of oxalic acid was studied in a well-mixed batch photoreactor (100 mm internal diameter, 120 mm height) containing aqueous suspensions of the semiconductor materials at a concentration of 1 g/L except for the case of WO_3 and Au/WO_3 samples, whose concentration was 0.04 g/L (Table 1). Oxalic acid as model substrate was selected as it decomposes to CO_2 and water following relatively simple reaction kinetics with no major intermediates [34]. Therefore, the reaction could be followed by a TOC analyzer. Each catalyst was dispersed in the aqueous solution in advance by sonication for 20 min and then transferred to the reactor vessel and stirred magnetically. Oxalic acid from a stock solution was then added to achieve an initial concentration of 1.8×10^{-2} mol/L, equivalent to 430 ppm TOC. Such a high initial concentration of oxalic acid was selected to ensure saturation of the surface of the photocatalyst with oxalic acid, to minimize the possibility of mass transfer limitations of oxalic acid from the bulk liquid [35] to the catalyst surface, and to allow the comparison of the activities of the semiconductor materials under identical experimental conditions. The initial volume of the irradiated reaction mixture was 350 ml. Oxygen was bubbled continuously at a flow rate of 12 $dm^3\ h^{-1}$ and the suspension was then left in the dark for 60 min, at 293 K, pH = 4 and atmospheric pressure, to achieve equilibrium conditions. Previous experimental runs [21,22] had shown that under the above experimental conditions the aqueous solutions were saturated with dissolved oxygen and that the oxalic acid decomposition reaction was not limited by mass transfer. The photoreactor was equipped with a halogen lamp (Tungsram, 500 W) for visible light irradiation and with a 9 W lamp (Philips PL-S 2P) for UV-A irradiation which were used either separately or in combination. The UV-A lamp was located inside a quartz tube, situated horizontally and immersed in the middle of the reactor suspension. The visible light lamp was located 12 cm above the

Table 1
Physical properties of the photocatalyst samples and zero-order reaction apparent rate constants (k_{app}).

Catalyst Sample	Oxide content (g/L)	BET surface area (m^2/g)	Average gold particle size (nm) ± 10%	Adsorption of oxalic acid (μmol/g catalyst)	k_{app} (λ = 365 nm) (mmol/L min) ± 5%	k_{app} (λ > 400 nm) (mmol/L min) ± 5%	k_{app} (UV + vis) (mmol/L min) ± 5%
None	–	–	–	–	0.0002	No	0.0002
TiO_2	1.0	50	–	420	0.040	0.0002	0.040
WO_3	0.04	10	–	388	0.0021	0.0024	0.0026
WO_3/TiO_2	0.04/0.96	45	–	396	0.058	0.004	0.058
Au/TiO_2	1.0	48	5	326	0.077	0.0003	0.077
Au/WO_3	0.04	10	6	322	0.0047	0.0049	0.0054
$Au/WO_3/TiO_2$	0.04/0.96	43	5	316	0.128	0.096	0.13

surface of the liquid in the reactor. A 400 nm cut-off glass filter (Schott) was used to remove the radiation in the UV region emitted by the halogen lamp. The photon flux in the visible light region at the surface of the liquid was 38 mW/cm^2, determined with a YSI 9100 Photometer (Thermo Fisher Scientific). The photon flux in the UV-A light region at the external wall of the quartz tube was 10 mW cm^{-2}, determined with a Microprocessor-Controlled Radiometer (Cole Parmer, 97503-00) fitted with 365 nm sensor. Samples collected at regular time interval during the dark period and during irradiation were filtered and the degree of mineralization of oxalic acid was assessed by means of a TOC analyzer, as described above.

3. Results and discussion

It is well known that catalyst specific surface area, degree of crystallinity and size of metal clusters on the catalyst surface can affect significantly the efficiency of photodestruction of water contaminants [18,21,22,33,36]. The specific surface areas of the semiconductor materials prepared are shown in Table 1. The surface area of WO_3 (10 m^2/g) was 5-fold less than the area of TiO_2 (50 m^2/g) and the surface area of the composited material WO_3 (4%)/TiO_2 (96%) (45 m^2/g) corresponded to the contribution of the two phases in accordance to their respective loading. The gold modified (0.4 wt% Au^0) materials, Au/WO_3, Au/TiO_2 and $Au/WO_3/TiO_2$ showed negligible change in the specific surface areas compared to the parent oxides. However, gold doping affected the adsorption of oxalic acid (in the dark) significantly, with a reduction of 17–22% of the equilibrium adsorption capacity with respect to the un-doped oxides (Table 1). This effect has been associated with a reduction of the external surface area of TiO_2 or WO_3 available for adsorption of oxalic acid as demonstrated in previous works [18,21,22].

Studying the coupled WO_3/TiO_2 systems by physical–chemical and spectroscopic methods it has been found out [25,28] that the band-gap energy of the composite WO_3/TiO_2 is lower than that of WO_3. UV–vis diffuse reflectance spectra were used to evaluate the band-gap energy of the bi-component WO_3/TiO_2 material and compare it with the respective energies of the pure TiO_2 and WO_3 materials. These spectra are represented in Fig. 1. It can be seen that the absorption edge for the WO_3/TiO_2 composite sample is shifted toward visible region compared to that of the pure TiO_2 and WO_3. The obtained results are in accordance with those obtained by some other authors [25,28,30] showing that the red shift in the absorption edge of the TiO_2/WO_3 composite depends on the method of synthesizing the photocatalyst sample, the nature of the precursors and on the temperature of calcinations of the samples [37]. For the samples under consideration the main absorption edge (λ_{ab}) for WO_3 sample is estimated to be 450 nm, while that for the WO_3/TiO_2 composite sample is found to be about 470 nm (Fig. 1). The measured band-gap energies of the samples by the described methods [38–40] are respectively for $WO_3 \approx 2.75$ eV and for the WO_3/TiO_2 composite sample ≈2.64 eV. The supposed explanation for the band-gap energy change in WO_3/TiO_2 composite sample is

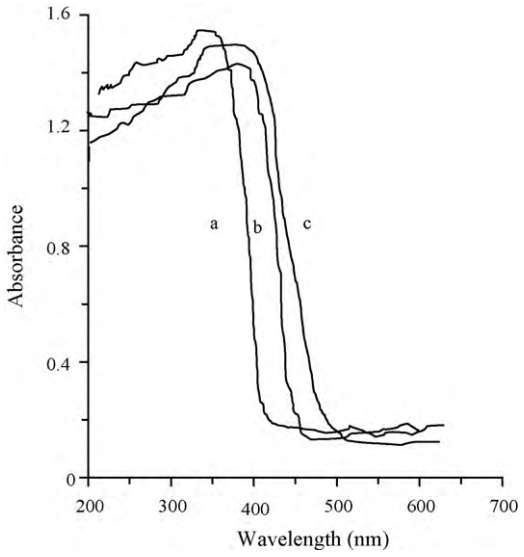

Fig. 1. UV–vis diffuse reflectance absorption spectra of samples: a: TiO_2; b: WO_3; c: WO_3/TiO_2.

based on formation of defect energy levels within the forbidden band of the TiO_2 and WO_3 [25].

The well-defined crystalline structure of the synthesized WO_3 was confirmed by the XRD studies of the samples (Fig. 2). The sharp peaks observed at $2\theta = 24.2^\circ$, 34.2°, 49.8° and 55.8° were indicative of the monoclinic WO_3 [41]. The XRD pattern of the bi-component WO_3/TiO_2 composite did not supply any new information, as the crystalline structure of the tungsten trioxide did not differ from that of the individual WO_3. This was also evidenced by the XPS peaks of WO_3, comprised in the WO_3/TiO_2 material (W $4f_{5/2}$, W $4f_{7/2}$) (Fig. 3A) proving the presence of WO_3 phase. The binding energy of W $4f_{7/2}$ (35.9 eV) corresponds to that characteristic of WO_3 (W^{6+} coordinated by oxygen atoms) (Fig. 3A) [42]. The morphological and structural differences of both WO_3 and WO_3/TiO_2 samples by SEM analysis are shown in Fig. 4A and B. TEM picture of the semiconductor materials (Fig. 4C) evidences that the average size of the WO_3

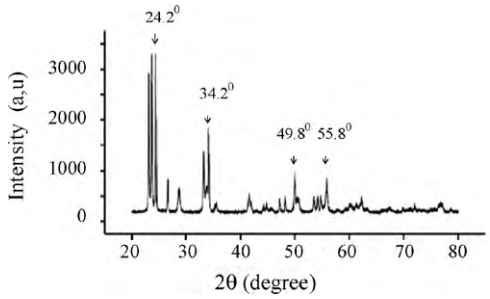

Fig. 2. XRD analysis of tungsten oxide.

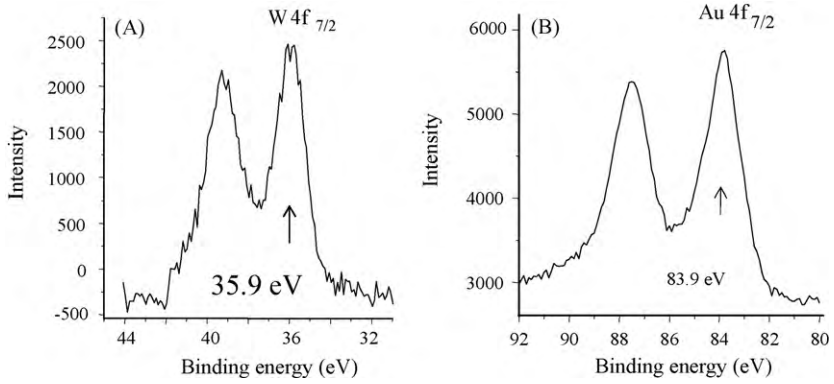

Fig. 3. XPS spectra of: (A) WO_3 in WO_3/TiO_2 composite; (B) Au modified WO_3/TiO_2.

crystallites comprised in the WO_3/TiO_2 material was 20 nm, which was about the same size as found in the individual WO_3 material.

The XPS spectra of Au modified TiO_2, reported in our previous studies, showed that the $AuCl_4^-$ adsorbed on the surface of the TiO_2 was photoreduced into metallic Au^0 nanoparticles attached on the surface of the oxide [21,22]. The binding energies of Au XPS peaks (Au $4f_{5/2}$ and Au $4f_{7/2}$) positioned at 87.6 and 83.9 eV, demonstrate that the superficially attached gold was completely reduced to metallic Au^0 (Fig. 3B). Therefore, the Au particles in the composite were deposited both on the TiO_2 and on the WO_3 and no other additional XPS peaks were registered and no broadening of the existing lines was observed.

In the case of photoreduction of $HAuCl_4$ on the surface of TiO_2, the pH of the medium exerts a remarkable influence on the size and quantity of gold nanoparticles deposited on the support [22,32]. In this work, the deposition of Au nanoparticles on the surface of the supports by photoreduction of the precursor $HAuCl_4 \cdot 3H_2O$ was carried out at pH = 7, for the reasons explained earlier. TEM analysis shows the size of gold nanoparticles, deposited on WO_3/TiO_2 (Fig. 4D). The average sizes of the Au particles on the semiconductor materials (Table 1) were 5 nm on Au/TiO_2 and $Au/WO_3/TiO_2$ and 6 nm on Au/WO_3, respectively. Such a small difference in Au particles size was insignificant and within the magnitude of the experimental errors.

The reduction–oxidation potential of oxalic acid of about 1.1 V vs NHE [43] and the mineralization kinetics of oxalic acid proceeding without any major intermediates [34], made it a suitable model pollutant for investigating the properties of the obtained photocatalyst samples. Fig. 5 presents the kinetics of mineralization of oxalic acid with suspensions of the semiconductor materials irradiated with either UV-A or visible light irradiation. The observed kinetics was found to be zero-order, which is the consequence of the very high concentration of oxalic acid selected. In the absence of catalyst oxalic acid was not mineralized. As it was expected, TiO_2 and Au/TiO_2 (traces a and b in Fig. 5B) did not show any significant photocatalytic activity, when they were irradiated with visible light, due to insufficient band-gap energy ($\Delta E_{TiO2} \approx 3.2$ eV) of the exciting radiation. In contrast, the WO_3 and the Au/WO_3 materials showed only low activity under both UV and visible light irradiation. This is the result of the combined effect of lower specific surface area of the WO_3 compared to TiO_2, and the small catalyst loading in suspension (0.04 g/L). The latter was purposefully selected to match the WO_3 loadings in the composite WO_3/TiO_2 and $Au/WO_3/TiO_2$ materials. WO_3/TiO_2 was found to be more active than the individual photocatalysts WO_3 or TiO_2, both under UV or visible light irradiation. In all cases doping of the semiconductor materials with gold nanoparticles enhanced the rate of mineralization of oxalic acid compared to the un-doped samples, and more significantly in the case of $Au/WO_3/TiO_2$. The photocatalytic mineralization of oxalic acid catalyzed by WO_3/TiO_2 or $Au/WO_3/TiO_2$ proceeded at a significantly higher rate under UV-A irradiation than the rate under visible light (Table 1 and Fig. 5).

The rate of photocatalytic degradation of organic pollutants has often been described by the Langmuir–Hinshelwood rate equation, derived from a simple saturation kinetics mechanism [2,18,44,45]. Recently the fundamental validity of this general kinetic expression has been put to scrutiny by Ollis [46] who proposed that both the rate apparent constant k_r and the substrate binding constant K may depend on the photon flux. However, under the present experimental conditions of very high concentration of oxalic acid and constant UV or visible flux, the Langmuirian kinetic expression in Ollis [46] reduces to a pseudo zero-order rate equation on oxalic acid concentration. The rate is therefore independent of the oxalic acid adsorption coverage, [18,44,47] and the concentration of oxalic acid is:

$$C_0 - C_t = k_{app} t \quad (1)$$

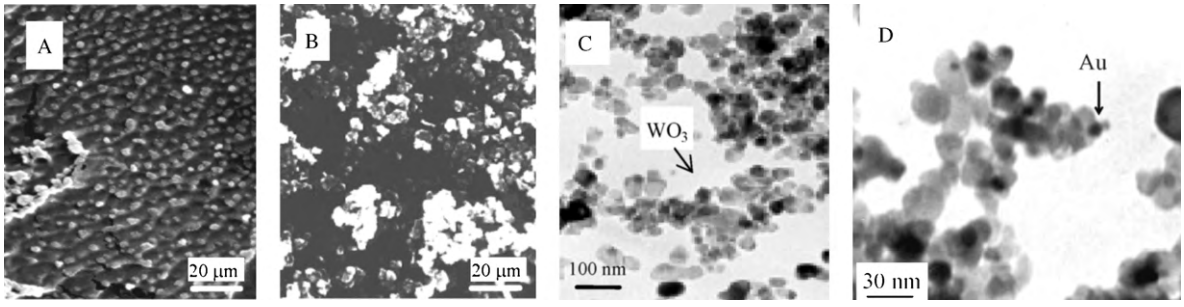

Fig. 4. (A) SEM micrograph of WO_3; (B) SEM micrograph of WO_3/TiO_2 composite; (C) TEM image of WO_3/TiO_2 composite; (D) TEM image of 0.4 wt% Au on WO_3/TiO_2 composite.

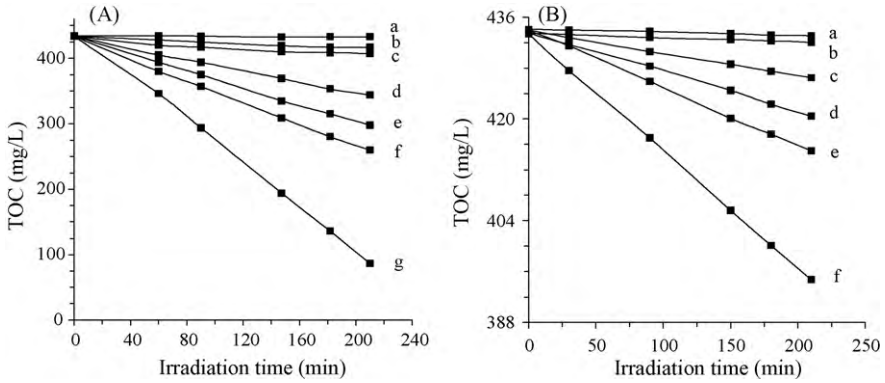

Fig. 5. Total degree of mineralization of oxalic acid (1.8×10^{-2} mol/L) at pH 4 by irradiation with: (A) UV light: a: absence of catalyst; b: WO_3; c: Au/WO_3; d: TiO_2; e: WO_3/TiO_2; f: Au/TiO_2; g: $Au/WO_3/TiO_2$; (B) visible light: a: TiO_2; b: Au/TiO_2; c: WO_3; d: WO_3/TiO_2; e: Au/WO_3; f: $Au/WO_3/TiO_2$.

where k_{app} is an apparent, zero-order, rate constant, C_0 is the initial concentration of the oxalic acid and C_t is the concentration as a function of time.

Fig. 6 shows the apparent rate constants of photocatalytic mineralization of oxalic acid with suspensions of the semiconductor materials irradiated with either UV-A, visible light, as well as, with combined UV-A and visible light irradiation. The rate constants with UV-A irradiation decrease in the following order: $Au/WO_3/TiO_2 > Au/TiO_2 > WO_3/TiO_2 > TiO_2 \gg Au/WO_3 > WO_3$, and with visible light irradiation they follow the order: $Au/WO_3/TiO_2 > Au/WO_3 > WO_3/TiO_2 > WO_3 \gg Au/TiO_2 \approx TiO_2$. Under UV-A irradiation the WO_3/TiO_2 photocatalyst showed a 0.45-fold increase in the rate of oxalic acid mineralization compared with the TiO_2 photocatalyst. However, more significant was the increase in the mineralization rates with the $Au/WO_3/TiO_2$ composite semiconductor material which was 3.2-fold higher than the rate with TiO_2 under UV-A irradiation and 2.2- to 2.4-fold higher than with the WO_3/TiO_2 material, under both UV-A and visible light irradiation. Similarly, the increase of the rate with Au/TiO_2 was 1.9-fold compared to the rate with TiO_2 under UV-A irradiation and with Au/WO_3 it was 2.0- to 2.2-fold higher compared to the rate with WO_3 under both UV-A and visible light irradiation. In summary, the results presented show that gold doping of the materials studied more than doubles the rates of mineralization of oxalic acid.

The initial steps in the photocatalytic processes occurring under irradiation of a semiconductor with photons of energy equal or greater than its band-gap have already been elucidated [48]. In the specific case of carboxylic acids, beside the direct destruction by the $HO^{\bullet}$ radicals generated on the valence band of the photocatalyst, there are also some additional anodic and cathodic processes [18,21,22,34,44] leading to the decomposition of the oxalic acid.

The photodecomposition of oxalic acid on the surface of WO_3/TiO_2 catalyst under UV-A irradiation is determined by several factors including the effectiveness of charge carrier separation in the photoexcited composite semiconductor material, the screening effect exerted by nanosized WO_3 particles on the surface of the photoactive TiO_2 surface and the adsorption capacity of the photocatalyst for oxalic acid. The screening effect of WO_3 on the surface of TiO_2 is confirmed by the TEM imaging (Fig. 4C) and loading higher than 4% usually results in the lowering of the photoactive surface area and therefore of the degradation rates of adsorbed organic compounds [26,30,49].

However, under optimal WO_3 loading, the increase in the rate constant of oxalic acid mineralization with the composite WO_3/TiO_2 catalyst can been explained in terms of an increased rate of charge carrier separation in the photoexcited composite catalyst as the dominating kinetic factor. A detailed explanation of the charge separation mechanism in the WO_3/TiO_2 composite photocatalyst has been reported [24,27]. The essence of the charge separation mechanism in the WO_3/TiO_2 photocatalyst consists in electron transfer from the conduction band of TiO_2 to the WO_3 conduction band, accompanied by consecutive W^{6+} reduction into W^{5+}, occurring on the surface of the WO_3 crystal lattice [24]. The electron transfer from the photoactive TiO_2 to WO_3 leads to an increase in the lifetime of the photogenerated pairs and as a consequence to a promotion of the photonic efficiency of the photocatalytic degradation of organic substrates (Fig. 7).

In the presence of visible irradiation WO_3 (E_{bg} = 2.8 eV), both as an individual photocatalyst and as a second component in the WO_3/TiO_2 composite, is excited. The rate constants of oxalic acid destruction under visible light irradiation were much lower than those registered under UV light illumination (Table 1), due to lower specific surface area of the WO_3 and its small amount (0.04 g/L). However, under visible light irradiation the rate constant of oxalic

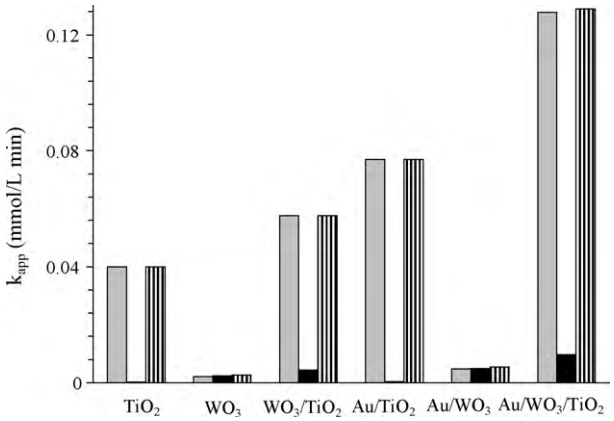

Fig. 6. Dependence of the apparent rate constants k_{app} of photocatalytic degradation of oxalic acid on the type of irradiation: ▭ – UV light; ■ – visible light; ▥ – combined UV–visible light.

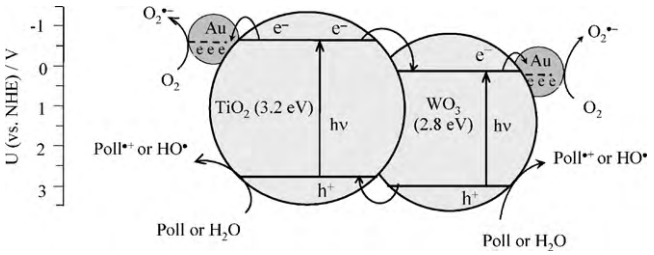

Fig. 7. Schematic representation of charge carrier separation in the photoexcited $Au/WO_3/TiO_2$ photocatalyst.

acid mineralization with the WO_3/TiO_2 composite was approximately double the rate measured with WO_3 (Table 1). In this case only the WO_3 phase is excited by visible light and the TiO_2 phase remain unexcited. The significant increase in photocatalytic activity of the composite WO_3/TiO_2 material comes as a result of the combined action of efficient separation of surface charge carriers in the composite (Fig. 7) and promotion of the acidity of the composite photocatalyst upon addition of WO_3. The increased acidity established in Refs. [24,50] generates a higher affinity towards adsorption of WO_3/TiO_2 for species with unpaired electrons, such as $O_2^{\bullet -}$, H_2O and HO^-. The increased adsorption of these species on the surface of the photocatalyst is aided by their higher local concentration in the vicinity of the surface. This favours the generation of $HO^\bullet$ radicals on the valence band and the reduction of O_2 on the conduction band of the WO_3/TiO_2 composite, and as a result the photonic efficiency of destruction of the oxalic acid is promoted additionally.

The rate constants of oxalic acid destruction increased in all cases (with UV or visible light irradiation) when the photocatalysts were doped with gold nanoparticles (Fig. 6). The effect of gold content and size of Au and other noble metals (Pt, Ag) nanoparticles on the photocatalytic activity of Au/TiO_2, Pt/TiO_2 and Ag/TiO_2 under UV light irradiation has been reported in our previous works [18,21,22]. It was shown there that increasing the size of the noble metal resulted in a decrease of photocatalyst activity. Upon exceeding the optimal gold loading on TiO_2 the efficiency of the photocatalytic process is decreased due to lowering of the adsorption capacity [21]. It was shown there that upon increasing the size of the gold particles, attached to the TiO_2 surface the activity of the photocatalyst is decreased [22]. In the case of irradiation with visible light, the rate constant of oxalic acid decomposition, catalyzed by Au/WO_3, was also increased by the doping compared to the parent WO_3 oxide (Fig. 6). We propose to explain the difference in the total rates of oxalic acid photooxidation based on the differences in the rates of the elementary steps in the presence and in the absence of the noble metal. In the case of band-gap excitation of single oxide semiconductor photocatalysts, a major rate-limiting factor controlling the photocatalytic efficiency [48,51] is the high degree of recombination between photogenerated electrons and holes. However, deposits of nanosized gold particles on the surface of the photocatalysts lead to an efficient charge separation of the photon generated electron–hole pairs in semiconductor photocatalysts and, therefore, to an increase in the lifetime of the photogenerated pairs. This allows longer time intervals for the charges to diffuse to the surface and to enable redox processes on the valence band and on the conduction band of the photocatalysts [34,51,52]. Noble metal nanoparticles are highly effective traps for the electrons due to the formation of a Schottky barrier at the metal–semiconductor contact.

Additional delocalization of the photoexcited electron on Au nanoparticles, attached to the photoinactive oxide in the WO_3/TiO_2 composite catalyst can be accomplished upon illumination with UV or visible light (Fig. 7). The influence of improved charge separation in the $Au/WO_3/TiO_2$ is evidenced by an increase in the rate constant of oxalic acid mineralization under UV, visible or combined UV–vis light irradiation which occurs despite a reduction of the oxalic acid absorption capacity (Table 1). Upon irradiation with UV light, the simultaneous excitation of both TiO_2 and WO_3 phases is accomplished in the coupled $Au/WO_3/TiO_2$ materials since the photon energy $E_{h\nu}$ is higher than the band-gap energies of the semiconductors. The rate constants of oxalic acid destruction for this reason are very close to those observed in the case of combined UV–vis light irradiation (Fig. 6). When the $Au/WO_3/TiO_2$ composite is irradiated with visible light, only the WO_3 phase is activated. The charge separation results from formation of Schottky barriers at the WO_3/TiO_2 contact surface and also at the Au/oxide interphase. The separation is further enhanced by the transfer of photogenerated electrons from the conduction band of WO_3 to TiO_2 followed by localization of the electrons on the gold nanoparticles. As a result, a significant increase in the photonic efficiency of the catalytic process is occurring. Especially efficient is the charge separation in the $Au/WO_3/TiO_2$ material upon irradiation with UV light or combined UV–visible light (Fig. 7). In this case the rate constants of oxalic acid decomposition were approximately 1.7 times higher than the constants with Au/TiO_2 material and three times higher than those catalyzed by pure TiO_2 (Table 1).

4. Conclusions

1. The rate constants of oxalic acid destruction (k_{eff}) under UV irradiation are much higher than those registered under visible light irradiation. The high values of the rate constants of oxalic acid decomposition upon irradiation with UV light are the results of the photocatalytic processes occurring simultaneously on TiO_2, WO_3 and coupled photocatalyst (photon energy $E_{h\nu} \geq$ band-gap energies of the semiconductors). Under illumination with visible light the WO_3 and the composite WO_3/TiO_2 photocatalyst do not manifest any high activity owing to the low specific surface area and low amount of WO_3 (4 wt%.).
2. The higher rate constant of photodestruction of the substrate catalyzed by WO_3/TiO_2 in comparison to the constants for the individual oxides can be attributed to the more efficient separation of surface charge carriers in the WO_3/TiO_2 photocatalyst and to an increase in the quantity of generated $HO^\bullet$ radicals on the valence bands of WO_3 and TiO_2, comprised by the composite photocatalyst as a result of the better adsorption of H_2O and HO^- on its surface.
3. The higher rate of photocatalytic destruction of oxalic acid in the case of deposited nanosized Au particles on the surface of the catalysts is owing to a more efficient charge separation, increase in the lifetime of the charge carriers and enhancement of the efficiency of the interfacial charge transfer to adsorbed substrates. Especially efficient is the charge separation in the case of the $Au/WO_3/TiO_2$ photocatalyst during irradiation with UV or combined UV–vis light, when the rate constants of oxalic acid destruction are approximately 1.7 times higher than that of the process catalyzed by Au/TiO_2 and 3 times higher than that on pure TiO_2.

Acknowledgements

The authors gratefully acknowledge financial support by NATO, Programme “Science for Peace”, Contract SfP 982835 and by National Science Fund, Ministry of Education and Sciences of Bulgaria (Project DO 02-252).

References

[1] A. Fujishima, K. Hashimoto, T. Watanabe, TiO_2 Photocatalysis, Fundamentals and Applications, Bkc Inc., Tokyo, 1999.
[2] I. Poulios, E. Micropoulou, R. Panou, E. Kostopoulou, Appl. Catal. B: Environ. 41 (2003) 345.
[3] M. Muneer, M. Qamar, D. Bahnemann, J. Mol. Catal. A: Chem. 234 (2005) 151.
[4] G. Li Puma, P.L. Yue, Ind. Eng. Chem. Res. 41 (2002) 5594.
[5] A.V. Vorontsov, V.P. Dubovitskaya, J. Catal. 221 (2004) 102.
[6] A.J. Maira, W.N. Lau, C.Y. Lee, P.L. Yue, C.K. Chan, K.L. Yeung, Chem. Eng. Sci. 58 (2003) 959.
[7] V. Latour, T. Pigot, P. Mocho, S. Blanc, S. Lacomb, Catal. Today 101 (2005) 359.
[8] E. Pelizzetti, Sol. Energy Mater. Sol. Cells 38 (1995) 453.
[9] C. Karunakaran, R. Dhanalakshmi, Solar energy mater, Solar Cells 92 (2008) 588.
[10] D. Chatterjee, S. Dasgupta, J. Photochem. Photobiol. C: Photochem. Rev. 6 (2005) 186.
[11] C.G. Granqvist, Solar energy mater, Solar Cells 91 (2007) 1529.
[12] V. Iliev, L. Prahov, L. Bilyarska, H. Fischer, G. Schulz-Ekloff, D. Wöhrle, L. Petrov, J. Mol. Catal. A 151 (2000) 161.
[13] D. Chatterjee, A. Mahata, Catal. Commun. 2 (2001) 1.

[14] E. Marais, R. Klein, E. Antunes, T. Nyokong, J. Mol. Catal. A: Chem. 261 (2007) 36.
[15] T.L. Thompson, J.T. Yates, Chem. Rev. 106 (2006) 4428.
[16] A.V. Emeline, V.N. Kuznetsov, V.K. Rybchuk, N. Serpone, Int. J. Photoenergy (2008) 19, Article ID 258394.
[17] S. Livraghi, M.C. Paganini, E. Giamello, A. Selloni, C. DiValentin, G.-F. Pacchioni, J. Am. Chem. Soc. 128 (2006) 15666.
[18] V. Iliev, D. Tomova, L. Bilyarska, A. Eliyas, L. Petrov, Appl. Catal. B: Environ. 63 (2006) 266.
[19] C. Wang, J. Li, G. Mele, G.-M. Yang, F.-X. Zhang, L. Palmisano, G. Vasapollo, Appl. Catal. B: Environ. 76 (2007) 218.
[20] G. Mele, E. Garcià-Loȅez, L. Palmisano, G. Dyrda, R. Słota, J. Phys. Chem. C 111 (2007) 6581.
[21] V. Iliev, D. Tomova, R. Todorovska, D. Oliver, L. Petrov, D. Todorovsky, M. Uzunova-Bujnova, Appl. Catal. A: Gen. 313 (2006) 115.
[22] V. Iliev, D. Tomova, L. Bilyarska, G. Tyuliev, J. Mol. Catal. A: Chem. 263 (2007) 32.
[23] A. Sclafani, J.-M. Herrmann, J. Photochem. Photobiol. A: Chem. 113 (1998) 181.
[24] V. Keller, P. Bernhardt, F. Garin, J. Catal. 215 (2003) 129.
[25] D. Ke, H. Lin, T. Peng, X. Liu, K. Dai, Mater. Lett. 62 (2008) 447.
[26] V. Puddu, R. Mokaya, G. Li Puma, Chem. Commun. 45 (2007) 4749.
[27] K. Akurati, A. Vital, J.-Ph. Dellemann, K. Michalowa, T. Graule, D. Ferri, A. Baiker, Appl. Catal. B: Environ. 79 (2008) 53.
[28] X.Z. Li, F.B. Li, C.L. Yang, W.K. Ge, J. Photochem. Photobiol. A: Chem. 141 (2001) 209.
[29] H. Shinguu, M.M.H. Bhuiyan, T. Ikegami, K. Ebihara, Thin Solid Films 506/507 (2006) 111.
[30] A.K.L. Sajjad, S. Shamaila, B. Tian, F. Chen, Appl. Catal. B: Environ. 91 (2009) 397.
[31] M. Sun, N. Xu, Y.W. Cao, J.N. Yao, E.G. Wang, J. Mater. Sci. Lett. 19 (2000) 1407.
[32] M. Haruta, Catal. Today 36 (1997) 153.
[33] A. Orlov, D.A. Jefferson, N. Macleod, R.M. Lambert, Catal. Lett. 92 (2004) 41.
[34] C.B. Mendive, M.A. Blesa, D. Bahnemann, Water Sci. Technol. 55 (2007) 139.
[35] M.d.l.M. Ballari, R. Brandi, O. Alfano, A. Cassano, Chem. Eng. J. 136 (2008) 242.
[36] D. Hufschmidt, D. Bahnemann, J.J. Testa, C.A. Emilio, M.I. Litter, J. Photochem. Photobiol. A: Chem. 148 (2002) 223.
[37] G.R. Bamwenda, H. Arakawa, Appl. Catal. A: Gen. 210 (2001) 181.
[38] F. Sanchez, T. Lopez, Mater. Lett. 25 (1995) 271.
[39] A.B. Murphy, Sol. Energy Mater. Sol. Cells 91 (2007) 1326.
[40] C.-F. Lin, C.-H. Wu, Z.-N. Onn, J. Hazard. Mater. 154 (2008) 1033.
[41] H. Tada, A. Kokrubu, M. Iwasaki, S. Ito, Langmuir 20 (2004) 4665.
[42] S. Penner, X. Liu, B. Klötzer, F. Klauser, B. Jenewein, E. Bertel, Thin Solid Films 516 (2008) 2829.
[43] K. Scott, H. Cheng, J. Appl. Electrochem. 32 (2002) 583.
[44] N. Serpone, J. Martin, S. Horikoshi, H. Hidaka, J. Photochem. Photobiol. A: Chem. 169 (2005) 235.
[45] E. Kusvuran, S. Irmak, B. Gozmen, O. Erbatur, Appl. Catal. B: Environ. 58 (2005) 211.
[46] D.F. Ollis, J. Phys. Chem. B 109 (2005) 2439.
[47] H. Tahiri, N. Serpone, R. Le van Mao, J. Photochem. Photobiol. A: Chem. 93 (1996) 199.
[48] M.R. Hoffmann, S.T. Martin, W. Choi, D.W. Bahnemann, Chem. Rev. 95 (1995) 69.
[49] H. Goĭmez, F. Orellana, H. Lizama, H.D. Mansilla, E.A. Dalchiele, J. Chilean Chem. Soc. 51 (2006) 1006.
[50] T. Onfroy, V. Lebarbier, G. Clet, M. Houalla, J. Mol. Catal. A: Chem. 318 (2010) 1.
[51] A.L. Linsebigler, G.Q. Lu, J.T. Yates, Chem. Rev. 95 (1995) 735.
[52] V. Subramanian, E.E. Wolf, P.V. Kamat, Langmuir 19 (2003) 469.